Reprinted from Nature, Vol. 316, No. 6029, pp. 596-601, 15 August 1985

A phage repressor–operator complex at 7 Å resolution

John E. Anderson, Mark Ptashne & Stephen C. Harrison

Department of Biochemistry and Molecular Biology, Harvard University, 7 Divinity Avenue, Cambridge, Massachusetts 02138, USA

The crystal structure of a complex between the DNA-binding domain of phage 434 repressor and a synthetic 434 operator shows that the protein, very similar in conformation to λ repressor, binds to B-form DNA with the second α-helix of a helix–turn–helix motif lying in the major groove.

WE present the X-ray crystal structure at 7 Å resolution of a repressor protein bound to its operator DNA. The protein (also a positive regulator of gene expression) is the amino-terminal, DNA-binding domain of the repressor encoded by coliphage 434, a close relative of phage λ. The operator is a 14-base-pair (bp) synthetic oligonucleotide with 2-fold symmetry that is specifically recognized by 434 repressor. Determination of the structure was facilitated by the preparation of isomorphous repressor-DNA crystals using operator DNA with 5-bromodeoxyuridine instead of thymine at two symmetry-related positions. Important aspects of the structure include: (1) The repressor conformation, predominantly α-helical, is remarkably similar to that of the first four α-helices of λ repressor[1]. (2) The DNA conformation is B-like, with some deviation at the ends of the operator. (3) Repressor contacts the DNA backbone at several distinct points. Bushman *et al.*[2] elsewhere in this issue present evidence that these are sites of strong interaction between repressor and DNA phosphates. (4) An α-helix (α3) lies in the major groove of the DNA and another α-helix (α2) lies across the groove. The helices α2 and α3 correspond to the helix-turn-helix motif found in the crystal structures of three other DNA-binding proteins[1,3,4] (and postulated to occur in many more, including 434 repressor[5–7]). The mode of binding to DNA is similar to that proposed for those proteins on the basis of model building[1,8–10,22], with the α3 helix disposed so that its residues can make sequence-specific contacts with DNA. Changing these residues in the α3 helix of 434 repressor can change the specificity of the repressor (ref. 11 and accompanying paper[12]).

Structure determination

Crystals of the complex of the 434 repressor DNA-binding domain R1-69 and synthetic 434 operator DNA were prepared as described previously[13]. The space group is I422, with $a = b = 166.4$ Å, $c = 139.4$ Å. Each strand of the synthetic DNA operator had the sequence 5′HO-d(A-C-A-A-T-A-T-A-T-A-T-T-G-T)-OH 3′. Derivative crystals were also prepared, using a similar oligonucleotide with 5-bromodeoxyuridine instead of dT at position 7. (Both 14mers were purchased from Pharmacia P-L Biochemicals.) Data were collected to 7 Å resolution using a Xentronics imaging proportional counter[14] with CuKα radiation from an Elliott GX-6 rotating anode X-ray generator. Integrated intensities were obtained as described by Durbin *et al.*[14] and processed using programs from P. R. Evans (MRC Laboratory of Molecular Biology, Cambridge, UK). Combination statistics are shown in Table 1. The mean isomorphous difference was small (0.12 for 1,105 common reflections). The consequent noisy difference Patterson could not be interpreted directly, but the positions of the Br atoms were obtained by a procedure that took advantage of the previously described analysis of packing in these crystals[13].

Table 1 Data combination statistics

	R_{sym}	N	$\bar{I}$
Native	0.087	1,171	270
Br	0.066	1,134	455

N, number of measurements; $\bar{I}$, mean intensity; $R_{sym} = \sum_h |\bar{I}_h - I_h| / \sum_h I_h$.

Protein-DNA complexes in the I422 crystals are stacked in rods with noncrystallographic 3_1 symmetry, parallel to the body diagonals of the unit cell. The rise per repeat of the 3_1 axis is 45.6 Å, so that the section of the difference Patterson perpendicular to the body diagonal and intersecting it 45.6 Å from the origin is a 'noncrystallographic Harker section', in the sense that it contains peaks representing vectors between atoms related by the noncrystallographic symmetry. On this section of the Patterson, we therefore expected to find a set of 3-fold-related peaks corresponding to vectors between Br atoms on different 14mers. Moreover, the known chemical structure of the derivative restricted the range of possible distances of these peaks from the noncrystallographic symmetry axis. Figure 1 shows the pattern actually found, before and after 3-fold averaging. It is similar to the pattern expected on the basis of the packing model of Anderson *et al.*[13], in which the DNA is stacked end-to-end in straight rods parallel to the unit cell body diagonals, but the peaks are ~5 Å farther from the axis than predicted. We found that B-DNA with a slight right-handed supertwist placed Br atoms in positions that matched the observed

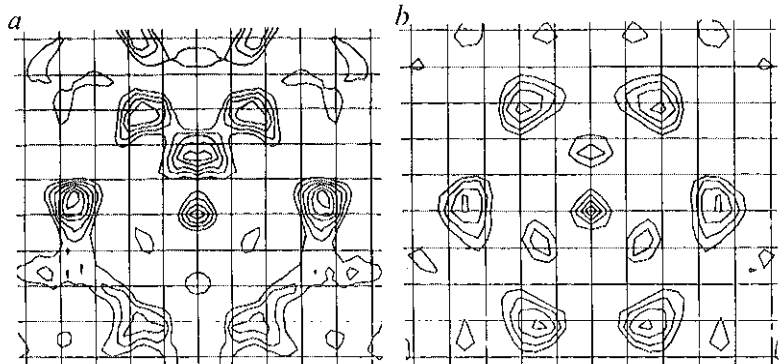

Fig. 1 Noncrystallographic Harker section. *a*, The section of the difference Patterson that lies 45.6 Å from the origin and perpendicular to the body diagonal of the unit cell. The body diagonal intersects the section at its centre. The small squares of the grid are 5 Å on a side. The set of six peaks corresponding to vectors between equivalent Br atoms on adjacent 14mers forms a roughly hexagonal array, with each peak lying ~18 Å from the body diagonal. Peaks from analogous Br atoms on straight B-DNA with its helix axis coincident with the body diagonal would lie 9.5 Å from the centre. *b*, The same section after 3-fold averaging about the body diagonal, using the programs of Bricogne[18].

Table 2 Br atom position refinement

Resolution (Å)	N	m	f_{rms}/E_{rms}	R_K
13.12–11.67	143	0.46	1.74	0.045
11.67–10.50	189	0.42	1.58	0.061
10.50–9.55	260	0.45	1.75	0.059
9.55–8.75	306	0.42	1.56	0.058
8.75–8.08	362	0.43	1.58	0.078
8.08–7.50	377	0.39	1.53	0.082
7.50–7.00	407	0.38	1.40	0.132
13.12–7.00	2,028	0.42	1.55	0.075

Comparison of initial and refined Br atom positions

Site	Initial	Refined	Occupancy
1	(0.16, −0.20, −0.01)	(0.161, −0.195, −0.013)	0.903
2	(−0.03, −0.26, 0.19)	(−0.033, −0.259, 0.190)	1.001
3	(−0.02, −0.29, 0.23)	(−0.020, −0.289, 0.227)	0.788
4	(−0.21, −0.48, 0.27)	(−0.211, −0.480, 0.270)	0.781
5	(−0.24, −0.47, 0.31)	(−0.242, −0.467, 0.307)	0.960
6	(−0.31, −0.66, 0.51)	(−0.306, −0.661, 0.511)	0.905

Statistics were calculated after 10 cycles of phasing and refinement[15], using I422 data expanded to space group I222, starting with the positions calculated from model B-DNA with a right-handed supertwist ($\alpha = -12°$; ref. 21) of the C-7 atoms of the thymine in position 7 of the 14mer sequence. m, Figure of merit; f_{rms}, root-mean-square heavy atom structure factor; E_{rms}, root mean square lack of closure error; $R_K = \sum |F_{PH}^{obs} - F_{PH}^{calc}| / \sum |F_{PH}^{obs}|$.

pattern much better. The local tilt of the DNA in this model was 12°.

Assignment of the Br–Br vectors on the noncrystallographic Harker section gives coordinates of the Br positions relative to the 3_1 axis, but leaves undetermined one translational degree of freedom, the displacement of this noncrystallographic symmetry axis from the body diagonal of the unit cell. There is also one origin ambiguity (see Fig. 2). The ambiguity was resolved, and the translational displacement determined, using a search procedure in which calculated Br contributions and centric $|F_{der} - F_{nat}|$ were compared (by means of a correlation function) between 15 and 7 Å resolution. The details will be reported elsewhere (J.E.A., J. Moulai and S.C.H., in preparation). A peak in the correlation function gave a trial solution, which was refined by conventional methods[15] (Table 2).

Native phases were determined and used to compute an initial electron-density map, which was inspected on an Evans and Sutherland PS300 interactive graphics system using the program FRODO (ref. 16). The map was noisy and contained no easily recognizable features, but averaging with respect to the noncrystallographic 3_1 axis gave some indication of a double-helical DNA backbone and several rod-like features where protein was expected.

Phases were refined by exploiting the redundancy of information present in the noncrystallographic 3_1 symmetry[17,18]. In drawing the envelope required for phase refinement[17,18], it proved helpful to use a model map that included the N-terminal domain of λ repressor[1] and DNA as a guide. The model consisted of the coordinates of λ-repressor residues 17–85 (ref. 1) (to match the size of R1-69), positioned to fit a straight double helix of DNA aligned along the noncrystallographic 3_1, and, instead of straight DNA, the coordinates of the supertwisted DNA used to locate the Br atom positions, with its superhelix axis coincident with the noncrystallographic symmetry axis. Inspection of the electron density computed from 7 Å structure factors of this model helped us to recognize features of the averaged initial map around which to draw the envelope. A total of six cycles of phase refinement were performed. The statistics are shown in Table 3 and part of the final map in Fig. 3. The positions of Br atoms are shown as stippled cubes in

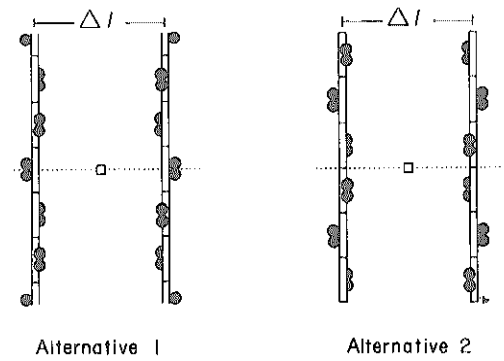

Fig. 2 Schematic projections down the 4-fold axis c (squares) of two of the four rods most closely associated with a lattice point, showing the two possible choices of origin (alternatives 1 and 2). The translational displacement, Δl (one of the parameters searched as described in the text) is shown for each. In alternative 1, the dyad between two Br atoms (filled circles) is coincident with the diagonal crystallographic dyad [110] (dotted line). In alternative 2, the dyad between two operators (rectangles) is coincident with the crystallographic dyad.

backbone are clearly visible, and it is easy to distinguish major and minor grooves. Rod-like density features (clearly low-resolution α-helices) are also visible next to the DNA on the opposite side from the Br atoms. One of these lies in the major groove of the DNA, and another is roughly at right angles to it. Their size and relative orientation show that they correspond to the helix–turn–helix motif seen in λ repressor[1], λ cro[3] and catabolite gene activator protein[4], and their position on the operator is consistent with modes of binding suggested for those proteins by model building[1,8–10,22].

Structure of R1-69

A backbone model for λ repressor[1] can be superimposed on the electron-density map of the co-crystal in such a way that α2 and α3 (the helix–turn–helix motif) are well aligned in rod-like density features (Fig. 4). Inspection shows that two other 'sausages' of density correspond closely to the α1 and α4 helices of λ repressor. The axis of the α1 density is displaced from the axis of the λ-repressor α1 helix by 2–3 Å, and its orientation is slightly different. The N-terminus of 434 repressor α1 density is close to the C-terminus of α3 density, and comparison with the λ repressor model suggests that it corresponds to the N-terminus of the polypeptide chain. The fit of the λ-repressor α4 helix to the co-crystal density is even closer than that of α1, although not quite as good as α2 and α3. The final helix of the λ-repressor domain (α5, not shown in Fig. 4) does not lie in clearly rod-like density, suggesting that the fold of the 434 repressor polypeptide chain differs significantly from the λ-repressor fold in this region. The λ-repressor helix α5 mediates a close dimer contact between N-terminal domains. Such

Table 3 Noncrystallographic symmetry phase refinement[18]

Cycle	R	r	Mean phase change
1	0.493	0.436	62.4°
2	0.397	0.618	17.2°
3	0.361	0.688	9.6°
4	0.340	0.732	7.4°
5	0.330	0.751	5.6°
6	0.324	0.761	3.9°
Overall phase change			68.9°

$R = \sum |F_{obs} - F_{calc}| / \sum |F_{obs}|$; mean phase change $= \sum |\phi_{calc} - \phi_{obs}| / N$;

$\sum |F_+ - |F_{++}| - \sum |F_{+-}| \sum |F_{calc}|$

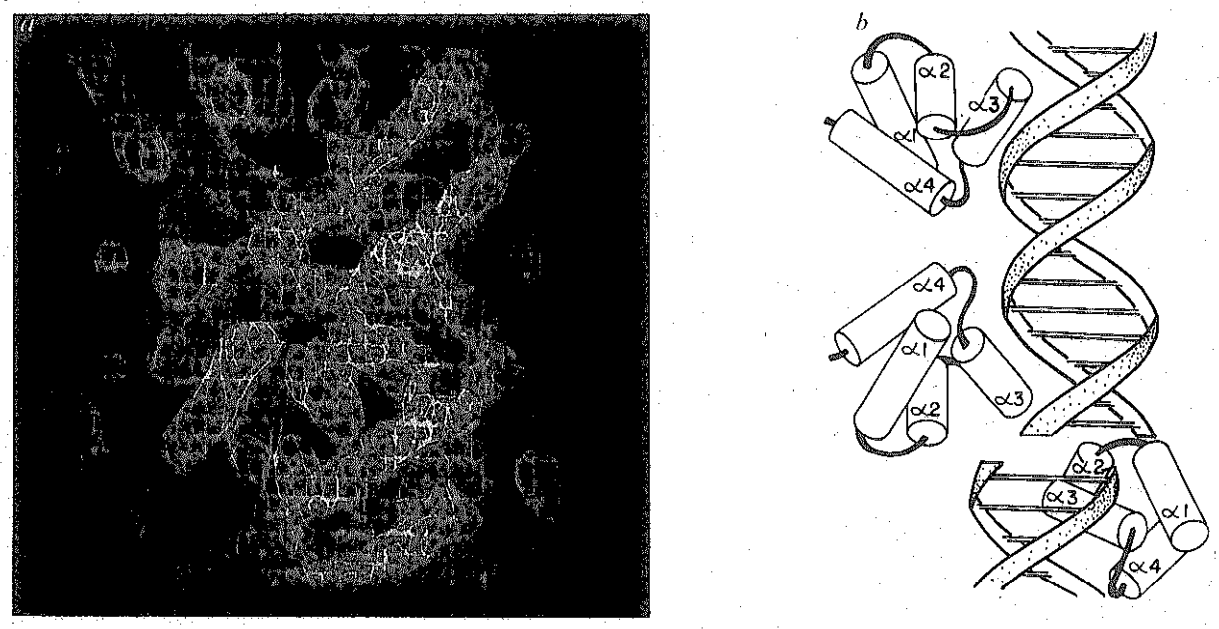

Fig. 3 *a*, Overview of the co-crystal map at 7 Å resolution after six cycles of noncrystallographic symmetry averaging and phase refinement. Almost an entire I422 asymmetric unit, consisting of three R1-69 monomers and one-and-a-half 14mers, is shown. Each protein–DNA complex consists of two protein monomers and one operator. The view is perpendicular both to the noncrystallographic 3_1 and to the dyad of a complex. The positions of Br atoms are shown as stippled spheres. Model B-DNA, tilted and displaced as described in the text, is superimposed on DNA electron density. *b*, Schematic representation of *a*, with α-helices (cylinders) labelled near their N-termini.

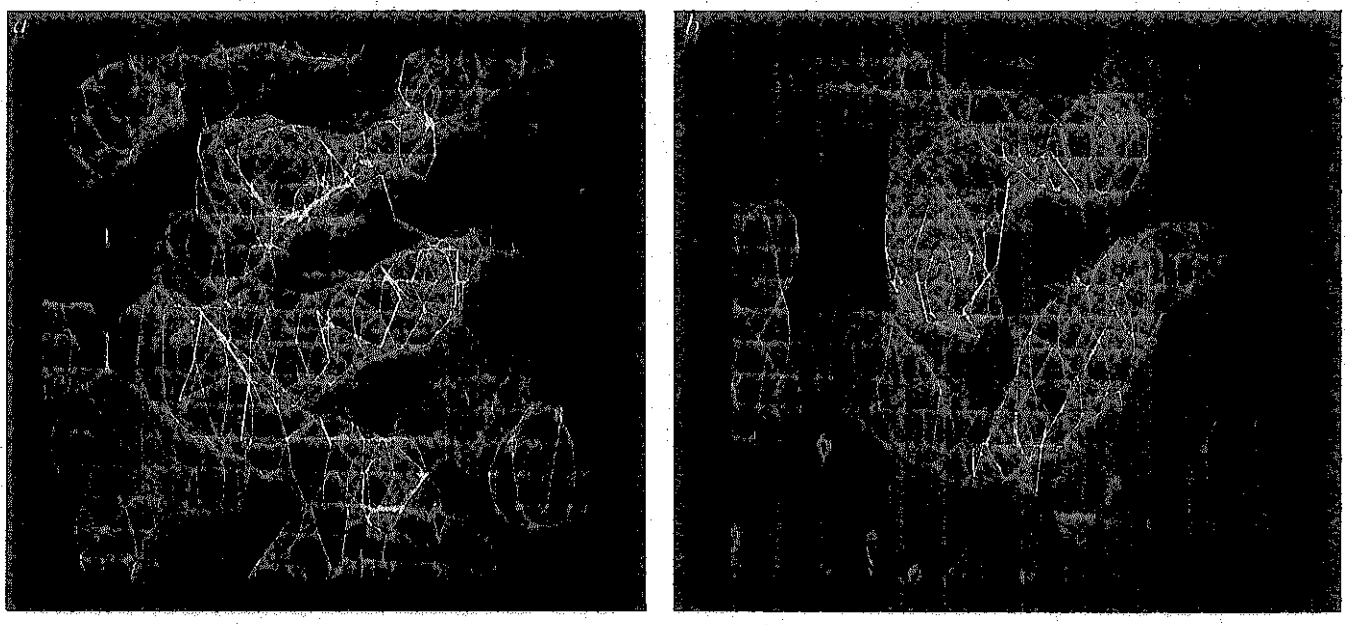

Fig. 4 Structure of R1-69. Straight B-DNA (red) and the α-carbon backbone of λ-repressor residues 17–75 (ref. 1) (gold), including the C-terminal half of α1 and all of α2–α4, are superimposed on the electron density (see text). *a*, View perpendicular to the noncrystallographic symmetry axis of part of a monomer of R1-69 (the lower one of the dimer in Fig. 3). Helix α3 lies in the major groove of the DNA and α2 lies across α3. A strong bridge of density connects the N-terminus of α2 to the DNA backbone near phosphate +14 (see Fig. 5*b* for phosphate numbering) of the adjacent 14mer. At the top, bridges between protein and DNA are partially visible near phosphates +9 and +10. *b*, View in the same orientation as *a*, but farther from the DNA, showing helices α1 (lower right) and α4 (upper left). Helices α2 and α3 are visible in the background. *c*, Schematic representation of *b*, with the α-helices (cylinders) labelled near their N-termini.

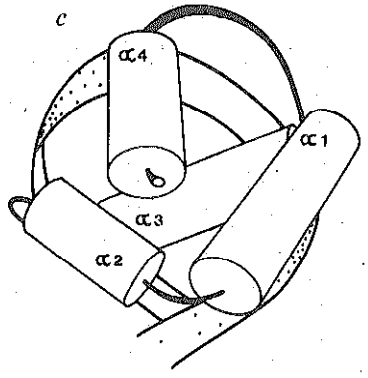

a close contact may indeed not occur in 434 repressor, because in the absence of DNA, R1-69 crystallizes as a monomer. (The space group of the R1-69 crystals is $P2_12_12_1$, with one protein molecule per asymmetric unit; S. Almo, J.E.A. and S.C.H., unpublished data.) The links between helices are not very clear in the co-crystal map (only the $\alpha 2$ and $\alpha 3$ 'sausages' are bridged by density at the level we chose to contour), but the correspondence between the λ-repressor model and rod-like density features makes us confident that we have correctly determined connectivity and chain direction. We conclude that R1-69 has a conformation very similar to that of the DNA-binding domain of λ repressor. It contains at least four α-helices, and their orientation and packing are similar in the two structures. The 434 repressor lacks the N-terminal arm of λ repressor, and the C-terminal portion of the domain may follow a different course.

Operator structure

Only the DNA backbone is clearly delineated at this resolution; density corresponding to base pairs is less regular. Ribbons of density follow fairly closely the path of the backbone of 10.5 bp per turn of B-DNA (Fig. 3), with a deviation of 2–3 Å towards the 3′ ends of each strand which is described below. The positions of the Br atoms indicate that the local axis of the DNA is displaced by a few ångstroms from the noncrystallographic 3_1 axis. In fitting the Br positions, we used a smooth supercoil with precise stacking of base pairs at the ends of adjacent 14mers, but the map suggests that a better fit can be obtained with a straight B-DNA model for each 14mer, tilted at ~12° with respect to the 3_1 and displaced from it by 4–5 Å, so that the register of the double helix is not maintained from 14mer to 14mer. This model produces nearly perfect overlap of the purine rings of the 5′ adenine bases from successive 14mers; the 3′ thymines are left unstacked. This exposure may in part account for the deviation of the 3′ end of the backbone density from the B-DNA model, and a contact with an R1-69 monomer bound to the adjacent 14mer may also be involved (see below). A perturbation of strict B-DNA structure to fit the density involves a displacement of the 3′ end of the 14-base strand by 2–3 Å (Fig. 5). As the 5′ end of the opposite strand is not correspondingly displaced, some distortion of normal base-pair geometry may be required to accommodate the backbone shift. The shift seems significant only for the four 3′-terminal bases.

Protein–DNA contacts

As shown in Figs 3, 4 and 5, R1-69 is bound to DNA with $\alpha 3$ inserted in the major groove, a feature anticipated by previous models of repressor–DNA interaction[1,3,4,8–10,22]. The axis of $\alpha 3$ is displaced by ~2 Å from the centre of the major groove. The position of the helix with respect to the base pairs seems to be determined by a set of contacts that the repressor domain makes with the DNA sugar–phosphate backbone (Fig. 5). One of these contacts is near the N-terminus of $\alpha 4$, where a strong bridge connects protein and DNA densities near the position of the phosphate 5′ to base +10. (For the numbering of phosphate groups, see Fig. 5.) A less striking bridge occurs near the adjacent phosphate, 5′ to base +9. Another strong bridge joins density from the N-terminus of $\alpha 2$ to density from the DNA backbone of the adjacent 14mer, near the phosphate between the two bases at the 3′ end of the strand. In phosphate ethylation interference experiments using the 14mer sequence embedded in continuous DNA, Bushman *et al.*[2] infer that corresponding phosphates are contacted by intact repressor in solution. Ethylation of the phosphates 5′ to bases −1 (the first base outside the 14mer sequence), +9 or +10 on either strand interferes strongly with repressor binding. We believe that the −1 phosphate contact corresponds to the contact in the crystal between $\alpha 2$ and the adjacent 14mer, and that the other two correspond to the bridges of density in the centre of the operator. These results show that the overall configuration of the complex of intact repressor with DNA is similar to that of R1-69, although it is possible that

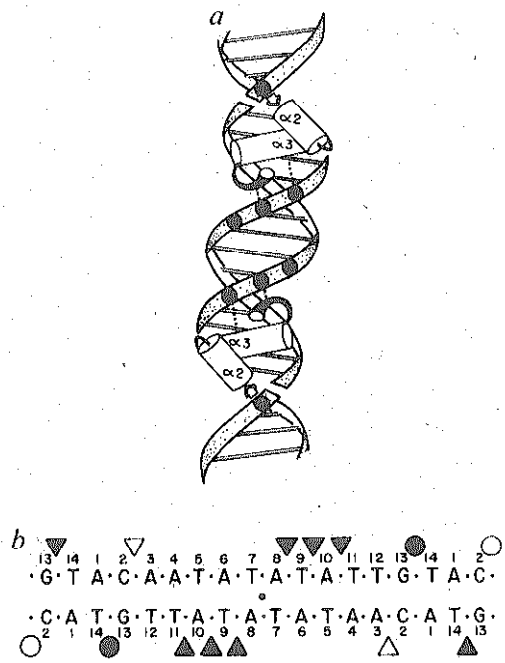

Fig. 5 Protein–DNA backbone contacts. *a*, Schematic drawing showing the contacts. The helix–turn–helix structures and part of the protein backbone just C-terminal to $\alpha 3$ are shown for a dimer of R1-69. The diagram includes one entire 14mer and the ends of the adjacent 14mers, drawn as straight B-DNA. The tilt of the adjacent 14mers is slightly exaggerated. Filled circles indicate positions where the locations of contacts between protein and DNA phosphates suggested by the crystal structure and those inferred from ethylation interference experiments[2] agree. Dotted lines connect the phosphates to the regions of the protein believed to provide the contacts. The part of the protein responsible for the phosphate contact nearest the centre of the operator is not known. The arrows show the directions of the displacements seen in the crystal of the 3′ ends of the DNA strands of the adjacent 14mers (see text). These displacements result in part from contacts made by the N-termini of the $\alpha 2$ helices of the dimer bound to the central 14mer. The corresponding displacements of the 3′ ends of the strands of the central 14mer, resulting from proteins bound to the adjacent 14mers, are not shown. *b*, The DNA sequence corresponding to *a*, showing the positions of possible contact between protein and DNA suggested by the crystal structure, and giving the phosphate numbering scheme used in the text. Bases belonging to the same 14mer are connected by small dots. The large dot in the centre locates the 2-fold axis of the central 14mer. Triangles, contacts made by the R1-69 dimer associated with the central DNA 14mer; circles, contacts made by proteins bound to the flanking 14mers. Filled symbols have the same meaning as in *a*; open symbols indicate positions where a contact is suggested by the crystal structure but not detected by ethylation interference[2].

the details of the interactions are slightly different because of constraints imposed by stable dimerization of the intact molecule.

Strictly speaking, confluences of protein and DNA densities such as those just described imply nothing more than close proximity, but it is reasonable to suppose that a bond will form if the appropriate type of residue is nearby. Groups most likely to interact directly with negatively charged DNA phosphates are those that are positively charged and those that can donate hydrogen bonds. Our confidence that we have correctly identified helices and their connectivity, and how they relate to the amino-acid sequence, permits us to enumerate amino-acid residues that could be involved in these interactions. We suggest that Asn 16 or Gln 17 (or both) might participate in the contact at the N-terminus of $\alpha 2$, Lys 40, Arg 41, or Arg 43 could be

involved in the +9 and +10 contacts; some residue C-terminal to $\alpha 4$ might also contact the +9 phosphate. We also note that helices $\alpha 2$, $\alpha 3$ and $\alpha 4$ are arranged so that the N-termini of all three point towards DNA phosphates. The N-terminus of an α-helix carries a virtual partial positive charge[19] which could produce favourable interactions with DNA phosphates to stabilize binding in the observed orientation. A role for interactions between the N-terminal ends of α-helices and backbone phosphates in the binding of λ repressor to DNA has been suggested previously[1].

With the relationship between protein and DNA in our interpretation of the electron density, it is not possible for Asn 16 or Gln 17 to hydrogen bond to the −1 phosphate if the operator is embedded in continuous, straight DNA. If the continuous DNA is given a slight supertwist, however, then both residues are brought to within reasonable hydrogen-bonding distance of the phosphate[2]. This suggests that if the ethylation interference at the −1 phosphate involves disruption of hydrogen bonds donated by Asn 16 or Gln 17, then the DNA is slightly bent (to a radius of curvature of ~100 Å) by repressor binding. A slight bend would also enhance any charge interaction that exists between the N-terminus of $\alpha 2$ (see above) and the −1 phosphate. Other deformations of the double helix are possible, but supertwisting (or bending) is the simplest and most easily interpretable. The displacement of 14mers from the noncrystallographic 3_1 axis, as well as the displacement of the 3′ end of the DNA strand seen in the crystal (see above and Fig. 5*a*), may be related to this suggested tendency of repressor to bend DNA when it binds[2]. A monomer of R1-69 bound to a particular 14mer in the crystal can make the $\alpha 2$ contact (which we propose is made to the −1 phosphate on bent continuous DNA in solution) only by lateral displacement of the neighbouring 14mer. The consequently unstacked 3′ end of this neighbour might then adjust further to optimize contact with the N-terminus of $\alpha 2$.

There are two other interactions between protein and DNA backbone suggested by our interpretation of the electron density. The N-terminus of $\alpha 3$ closely approaches the DNA backbone, placing the side chain of Ser 30 in a position to hydrogen bond to the phosphate 5′ to base +11. Ethylation at that phosphate decreases binding, although less strongly than the modifications described above[2]. Finally, just beyond the C-terminus of $\alpha 3$, an arm of density reaches towards the opposite DNA strand near the phosphate 5′ to base +3. The location and orientation of the arm suggest a salt bridge between that phosphate and the side chain of Lys 38, but ethylation at that position has little effect on binding[2].

Side chains on the external surface of $\alpha 3$ (those that would be exposed to the solvent if not in the complex) are clearly in position to make sequence-specific contacts to the bases in the major groove. The excellent fit of the λ-repressor backbone and of B-DNA to features of the electron density, the invariance in three other structures of the helix–turn–helix motif[5,20], and the assignment by sequence similarity of corresponding residues in the λ and 434 repressors[6,7] permit limited model building of specific interactions between protein and DNA by insertion of 434 repressor side chains onto λ-repressor backbone positioned as in Fig. 5. An important preliminary conclusion is that base pairs 1–4 seem to be accessible to direct interaction with repressor side chains on the $\alpha 3$ helix, with contacts possible between Gln 28 and base pair 1, Gln 29 and base pairs 2 and 3, and Gln 33 and base pairs 3 and 4. In addition, residues in the turn between $\alpha 3$ and $\alpha 4$ can probably contact base pair 5 and possibly base pair 6. We are attempting to test these suggestions and are extending the resolution of the structure determination to 3.2 Å.

We thank Javad Moulai for help in processing the data. We also thank Aneel Aggarwal, Rick Bushman, Karen Chapman, Michael Levitt, Jim Wang, Robin Wharton and Cynthia Wolberger for helpful comments. J.E.A. is a Burroughs Wellcome Fund Fellow of the Life Sciences Research Foundation. This work was supported by NIH grant GM29109 to S.C.H. and M.P.

Received 19 April; accepted 14 June 1985.

1. Pabo, C. O. & Lewis, M. *Nature* **298**, 443–447 (1982).
2. Bushman, F. D., Anderson, J. E., Harrison, S. C. & Ptashne, M. *Nature* **316**, 651–653 (1985).
3. Anderson, W. F., Ohlendorf, D. H., Takeda, Y. & Matthews, B. W. *Nature* **290**, 754–758 (1981).
4. McKay, D. B. & Steitz, T. A. *Nature* **290**, 744–749 (1981).
5. Steitz, T. A., Ohlendorf, D. H., McKay, D. B., Anderson, W. F. & Matthews, B. W. *Proc. natn. Acad. Sci. U.S.A.* **79**, 3097–3100 (1982).
6. Sauer, R. T., Yocum, R. R., Doolittle, R. F., Lewis, M. & Pabo, C. O. *Nature* **298**, 447–451 (1982).
7. Takeda, Y., Ohlendorf, D. H., Anderson, W. F. & Matthews, B. W. *Science* **221**, 1020–1026 (1983).
8. Ohlendorf, D. H., Anderson, W. F., Fisher, R. G., Takeda, Y. & Matthews, B. W. *Nature* **298**, 718–723 (1982).
9. Weber, I. T. & Steitz, T. A. *Proc. natn. Acad. Sci. U.S.A.* **81**, 3973–3977 (1984).
10. Ebright, R. H., Cossart, P., Gicquel-Sanzey, B. & Beckwith, J. *Proc. natn. Acad. Sci. U.S.A.* **81**, 7274–7278.
11. Wharton, R. P., Brown, E. L. & Ptashne, M. *Cell* **38**, 361–369 (1984).
12. Wharton, R. P. & Ptashne, M. *Nature* **316**, 601–605 (1985).
13. Anderson, J., Ptashne, M. & Harrison, S. C. *Proc. natn. Acad. Sci. U.S.A.* **81**, 1307–1311 (1984).
14. Durbin, R. *et al. Science* (submitted).
15. Dickerson, R. E., Weinzierl, J. E. & Palmer, R. E. *Acta crystallogr.* **B24**, 997–1003 (1968).
16. Jones, T. A. *J. appl. Crystallogr.* **11**, 268–272 (1978).
17. Bricogne, G. *Acta crystallogr.* **A30**, 395–405 (1974).
18. Bricogne, G. *Acta crystallogr.* **A32**, 832–847 (1976).
19. Hol, W. G. J., van Duijnen, P. T. & Berendsen, H. J. C. *Nature* **273**, 443–446 (1978).
20. Ohlendorf, D. H. Anderson, W. F., Lewis, M., Pabo, C. O. & Matthews, B. W. *J. molec. Biol.* **169**, 757–769 (1983).
21. Crick, F. H. C. *Acta crystallogr.* **6**, 685–689 (1953).
22. Lewis, M. *et al. Cold Spring Harb. Symp. quant. Biol.* **47**, 435–440 (1983).